Geometric Method of Fully Constrained Least Squares Linear Spectral Mixture Analysis

Liguo Wang, Danfeng Liu, and Qunming Wang

***Abstract*—Spectral unmixing is one of the important techniques for hyperspectral data processing. The analysis of spectral mixing is often based on a linear, fully constrained (FC) (i.e., nonnegative and sum-to-one mixture proportions), and least squares criterion. However, the traditional iterative processing of FC least squares (FCLS) linear spectral mixture analysis (LSMA) (FCLS-LSMA) is of heavy computational burden. Recently developed geometric LSMA methods decreased the complexity to some degree, but how to further reduce the computational burden and completely meet the FCLS criterion of minimizing the unmixing residual needs to be explored. In this paper, a simple distance measure is proposed, and then, a new geometric FCLS-LSMA method is constructed based on the distance measure. The method is in line with the FCLS criterion, free of iteration and dimension reduction, and with very low complexity. Experimental results show that the proposed method can obtain the same optimal FCLS solution as the traditional iteration-based FCLS-LSMA, and it is much faster than the existing spectral unmixing methods, particularly the traditional iteration-based method.**

***Index Terms*—Fully constrained (FC) least squares (FCLS), hyperspectral, linear spectral mixture analysis (LSMA), spectral unmixing.**

I. Introduction

In RECENT years, hyperspectral remote sensing has been studied extensively for various applications, ranging from land cover use and land cover change to target detection. Hyperspectral data analysis has become critical for extracting the rich information provided in the spectral measures for the imaged areas. Thematic maps are usually obtained by assigning each pixel to one of the defined ground cover types by applying an appropriate classification technique [1]. This is often referred to as hard or crisp classification. An issue in performing a hard classification is that there often exist a large number of mixed pixels due to the limited spatial resolution. To cope with this problem, soft classification techniques have been investigated, which analyze the proportions of primitive classes (endmembers) contained in each mixed pixel via spectral unmixing algorithms [2], [3]. Given all the endmembers or constituent spectra in a set of hyperspectral images, the task of spectral unmixing is to work out the abundance of each endmember within each pixel.

Spectral unmixing methods have been investigated for more than 20 years, and the linear spectral mixture model (LSMM) [3] is widely used for its clear physical meanings and the convenience of applications, by which a mixed pixel's reflectance is assumed to be a weighted sum of all the endmembers. In this model, each endmember's spectral characteristic is represented by a single spectrum, which may be acquired with unsupervised endmember extraction algorithms, such as N-FINDR, pixel purity index, and iterative error analysis, as reviewed and evaluated in [4], or derived from training data when they are available [5], [6].

The LSMM is often solved based on a least squares criterion. To make the outputs of linear unmixing meaningful and acceptable, two constraints are often imposed on the abundances of materials in a pixel: 1) abundance sum-to-one constraint (ASC) and 2) abundance nonnegativity constraint (ANC). A fully constrained (FC) least squares (FCLS) linear spectral mixture analysis (LSMA) (FCLS-LSMA) [7]–[15] simultaneously considers the ASC and the ANC. Although the ASC is easy to meet, the ANC, as well as the full constraint, is difficult to realize and usually requires iterative optimization methods, as the ANC results in a set of inequalities that cannot be solved analytically.

In past years, large efforts were devoted to solving FCLS linear unmixing problems. Shimabukuro and Smith [7] considered several constrained least squares mixing models and obtained constrained least squares solutions by solving an overdetermined system. Since there are no closed-form solutions, one must examine possible solutions in a feasible region bounded by the full constraints. The use of quadratic programming techniques to impose the full constraints was investigated in [8]–[10], but the algorithms were of great computational burden. The iteration-based method in [11] and [12] reduced the complexity of FC linear unmixing problems. It considers partially constrained least squares LSMA at first and then takes advantage of its solutions to solve FC linear mixing problems. Following this way, a suboptimal solution to the FCLS linear unmixing problem is obtained by the iterative method.

Alternatively, geometric methods were proposed to speed up the analysis of the linear unmixing problem. Geng *et al.* [13] proposed a geometric LSMA method to decrease the complexity of iteration-based LSMA. The volume of the simplex formed

Manuscript received June 23, 2011; revised September 6, 2012; accepted October 7, 2012. Date of publication December 21, 2012; date of current version May 16, 2013. This work was supported by the National Natural Science Foundation of China under Grant 61275010.

L. Wang and D. Liu are with the College of Information and Communications Engineering, Harbin Engineering University, Harbin 150001, China (e-mail: wangliguo@hrbeu.edu.cn; liudanfeng@hrbeu.edu.cn).

Q. Wang was with the College of Information and Communications Engineering, Harbin Engineering University, Harbin 150001, China. He is now with the Department of Land Surveying and Geo-Informatics, The Hong Kong Polytechnic University, Kowloon, Hong Kong (e-mail: wqm11111@126.com).

Color versions of one or more of the figures in this paper are available online at http://ieeexplore.ieee.org.

Digital Object Identifier 10.1109/TGRS.2012.2225841

by d vertexes of endmembers $\mathbf{e}_1, \mathbf{e}_2, \ldots, \mathbf{e}_d$ and original point $\mathbf{O}$ is given by

$$\mathrm{Vol}(\mathbf{O}, \mathbf{e}_1, \mathbf{e}_2, \ldots, \mathbf{e}_d) = \frac{1}{(d-1)!}\sqrt{|\mathbf{E}^{\mathrm{T}}\mathbf{E}|} \quad (1)$$

where $\mathbf{E} = [\mathbf{e}_1, \mathbf{e}_2, \ldots, \mathbf{e}_d]$ and $|\bullet|$ is the determinant operator. Then, we get the fractional abundance p_i by

$$p_i = \frac{\mathrm{Vol}_i}{\mathrm{Vol}_0} = \frac{\mathrm{Vol}(\mathbf{O}, \mathbf{e}_1, \ldots, \mathbf{e}_{i-1}, \mathbf{s}_0, \mathbf{e}_{i+1}, \ldots, \mathbf{e}_d)}{\mathrm{Vol}(\mathbf{O}, \mathbf{e}_1, \mathbf{e}_2, \ldots, \mathbf{e}_d)}, \quad i = 1, 2, \ldots, d. \quad (2)$$

Using (2) to obtain the abundances is free of iteration. However, the volume computation is still of heavy burden.

Similarly, the volume measure in [14] can also be used to solve LSMM. The volume of the simplex formed by d vertexes of endmembers $\mathbf{e}_1, \mathbf{e}_2, \ldots, \mathbf{e}_d$ is given by

$$\mathrm{Vol}(\tilde{\mathbf{E}}) = \frac{1}{d!}|\tilde{\mathbf{E}}| \quad (3)$$

where

$$\tilde{\mathbf{E}} = \begin{bmatrix} 1 & 1 & \cdots & 1 \\ \mathbf{e}_1, & \mathbf{e}_2, & \ldots, & \mathbf{e}_d \end{bmatrix}. \quad (4)$$

If we divide the geometric measures into two types, namely, positive measures (i.e., the value of the measures is always positive) and signed measures (i.e., the value of the measures may be either positive or negative), then volume case (3) can be classified as the signed type. Although the complexity of (3) is lower than that of (1), it is still high.

Wang *et al.* [15] and Wang and Zhang [16] constructed a distance measure, and it could take the place of the volume measure for LSMA to decrease the complexity.

In a $(d-1)$-dimensional data space, let $\mathbf{e}_1, \mathbf{e}_2, \ldots, \mathbf{e}_d$ be the d endmembers and $\mathbf{s}_0$ be a mixed pixel. The superplane formed by the vertexes of $\mathbf{e}_1, \mathbf{e}_2, \ldots, \mathbf{e}_{i-1}, \mathbf{e}_{i+1}, \ldots, \mathbf{e}_d$ is given by

$$\boldsymbol{\alpha}^{\mathrm{T}}(\bullet) + b = 0 \quad (5)$$

in which $\boldsymbol{\alpha} = (\alpha_1, \alpha_2, \ldots, \alpha_{d-1})^{\mathrm{T}}$ is the solution of the following equation:

$$[\mathbf{e}_1, \mathbf{e}_2, \ldots, \mathbf{e}_{i-1}, \mathbf{e}_{i+1}, \ldots, \mathbf{e}_d]^{\mathrm{T}} \cdot \boldsymbol{\alpha} + b \cdot \mathbf{I}_{d-1} = 0 \quad (6)$$

where $\mathbf{I}_{d-1}$ is a vector with a size of $(d-1) \times 1$. b takes zero if the original point is linearly correlated to $\mathbf{e}_1, \mathbf{e}_2, \ldots, \mathbf{e}_{i-1}, \mathbf{e}_{i+1}, \ldots, \mathbf{e}_d$ and one if otherwise. In practice, b has little chance to be zero. Then, the distance from $\mathbf{s}_0$ to the superplane (6) is given by

$$D(\mathbf{s}_0) = \boldsymbol{\alpha}^{\mathrm{T}}\mathbf{s}_0 + b. \quad (7)$$

The replacement greatly reduces the complexity of the geometric LSMA method. The weakness of the distance measure is that it can only be used in a reduced dimensional space, and the complexity of dimension reduction should not be omitted.

Luo *et al.* [17] proposed a distance measure that can be used in any dimensional space, but it is still time consuming. The distance $D(\mathbf{s}_0)$ from point $\mathbf{s}_0$ to the space spanned by $\widehat{\mathbf{E}}_i$ is then given by

$$D(\mathbf{s}_0) = \overline{\widehat{\mathbf{E}}}_i^{+}\overline{\widehat{\mathbf{E}}}_i \quad (8)$$

where $\widehat{\mathbf{E}}_i = [\mathbf{e}_1, \mathbf{e}_2, \ldots, \mathbf{e}_{i-1}, \mathbf{e}_{i+1}, \ldots, \mathbf{e}_d]$, $\overline{\widehat{\mathbf{E}}}_i$ is the base of null space $\widehat{\mathbf{E}}_i$, and $\overline{\widehat{\mathbf{E}}}_i^{+}$ is the Moore–Penrose generalized inverse matrix of $\overline{\widehat{\mathbf{E}}}_i$. Then, the fractional abundance p_i of $\mathbf{e}_i$ in pixel $\mathbf{s}_0$ can be obtained by $\|D(\mathbf{s}_0)\|_2 / \|D(\mathbf{e}_i)\|_2$, $i = 1, 2, \ldots, d$.

Geometric measures (3) and (7) can only be calculated in the $(d-1)$-dimensional space. The two popular dimension reduction methods are principal component analysis [18] and maximum noise fraction transform [19]. The preprocessing of dimensionality reduction adds the computation burden.

It is worth mentioning that [20] provided a good method to speed up the solving of FCLS-LSMA. However, the optimal least squares solution could not be obtained by this method for the use of an approximate assumption in it, as mentioned in this reference. Additionally, the implementation of zone determination increased the complexity of the method.

The aforementioned geometric measures can decrease the complexity of the iterative LSMA method to certain degrees, but they are often implemented in a subspace with dimension reduction.

Aside from complexity, another issue worthy of addressing for the aforementioned geometric LSMA methods is about the requirement for imposing abundance constraints. When a mixed pixel is within the convex, its fractional abundances obtained by each geometric method based on the measures in [13]–[17] are FC naturally. However, it is the case for a mixed pixel out of the convex. It is easy to know that the fractional abundances obtained by signed-measure-based methods just meet the ASC requirement while the abundances obtained by positive-measure-based methods just meet the ANC requirement. A simple way to meet full-constraint requirements is to set the negativity abundances to zero and the abundances more than one to one and then to divide each of the new abundances by the sum of them [13], [17], [21]. After this processing, the abundances are FC. However, this kind of processing is just to obtain the FC results and is not in line with the least squares criterion. A detailed analysis can be seen in Section III-B. In general, signed measures have lower unmixing error than positive ones under the abundance adjustment and can provide the spatial position information whether a mixed pixel is within the convex formed by the corresponding endmembers. For these reasons, the property of signed measures is better than that of positive ones, as shown in related discussions and the experiments later. In fact, signed measures can be used as positive ones, but no benefit will be gained.

In general, the iteration-based LSMA methods and the aforementioned geometric LSMA methods have disadvantages in terms of complexity and/or full-constraint requirements. In this paper, a new distance measure is proposed, and then, an effective geometric FCLS-LSMA method is constructed based on the distance measure. The complexity and unmixing performance of the proposed method are analyzed and compared with those of some typical existing methods.

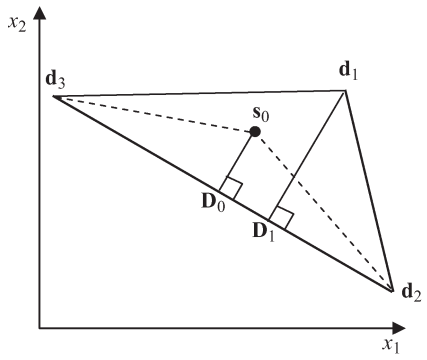

Fig. 1. Diagram of geometric LSMA.

The rest of this paper is organized as follows. Section II introduces the concept of the geometric LSMA method. Section III presents the geometric FCLS-LSMA method, including the construction of a new distance measure and the FC implementation of the geometric method. In Section IV, experiments are carried out to evaluate the performance of the geometric FCLS-LSMA method. Section V concludes this paper.

II. Geometric LSMA Method

Let N be the band number or data dimensionality and d be the class number or endmember number included in LSMA. Denote $\mathbf{E} = [\mathbf{e}_1, \mathbf{e}_2, \ldots, \mathbf{e}_d]$ as the $N \times d$ matrix which includes all endmembers $\mathbf{e}_1, \mathbf{e}_2, \ldots, \mathbf{e}_d$. Then, the LSMM can be expressed as

$$\mathbf{s}_0 = \mathbf{EP} + \boldsymbol{\varepsilon} \tag{9}$$

where $\mathbf{s}_0$ is the pixel spectrum to be unmixed, $\mathbf{P} = [p_1, p_2, \ldots, p_d]^{\mathrm{T}}$ is a set of fractional abundances, and $\boldsymbol{\varepsilon}$ is the unmixing residual. The least squares criterion indicates that the objective of unmixing is to obtain the optimal fractional abundances $\mathbf{P}$ corresponding to the minimum $\|\boldsymbol{\varepsilon}\|_2$. This criterion is employed throughout this paper. Under this condition, the optimal solution of modeling (9) has the following geometric explanation. For the purpose of visualization, a 2-D space is considered. In Fig. 1, $\mathbf{s}_0$ is mixed by endmembers $\mathbf{d}_1$, $\mathbf{d}_2$, and $\mathbf{d}_3$ with fractional abundances p_1, p_2, and p_3, respectively. Let S be the area of the triangle formed by $\mathbf{d}_1$, $\mathbf{d}_2$, and $\mathbf{d}_3$ and S_1 be the area of the triangle formed by $\mathbf{s}_0$, $\mathbf{d}_2$, and $\mathbf{d}_3$. Let $D(\mathbf{d}_1)$ and $D(\mathbf{s}_0)$ be the distances from $\mathbf{d}_1$ and $\mathbf{s}_0$ to line $\mathbf{d}_2\mathbf{d}_3$, respectively. Then, p_1, S_1, and S are linked by

$$p_1 = \frac{S_1}{S}. \tag{10}$$

Formula (10) can also be equally expressed by

$$p_1 = \frac{D(\mathbf{s}_0)}{D(\mathbf{d}_1)}. \tag{11}$$

Similarly, p_2 and p_3 can also be obtained by a ratio of areas or distances. The case is easy to be extended to a high-dimensional space, in which volume takes the place of area. It can be seen that one of the key contents of constructing a geometric LSMA method is to construct an effective volume or distance measure. A new distance measure is proposed in this paper and presented in the next section.

III. Geometric FCLS-LSMA Method

This section first presents a new signed distance and then constructs a geometric FCLS-LSMA method based on the proposed distance measure.

A. Construction of a Signed Distance Measure

1) Methodology: Let $\mathbf{s}_0$ be the pixel to be unmixed and $\mathbf{e}_1, \mathbf{e}_2, \ldots, \mathbf{e}_d$ be the endmembers. In order to estimate the d fractional abundances, d distances $f_i(\bullet)$, $i = 1, 2, \ldots, d$, with different directions should be constructed.

Suppose that $f_i(\bullet)$ $(i = 1, 2, \ldots, d)$ meets $f_i(\mathbf{e}_i) = 1$ and $f_i(\mathbf{e}_{j\neq i}) = 0$ and has the form of

$$f_i(\bullet) = \mathbf{k}_i^{\mathrm{T}}(\bullet) + b_i, \qquad i = 1, 2, \ldots, d \tag{12}$$

where super slope $\mathbf{k}_i$ $(i = 1, 2, \ldots, d)$ is a d-dimensional column vector and scalar quantity b_i $(i = 1, 2, \ldots, d)$ is a threshold value. Then, the following equation should be met:

$$\begin{cases} \mathbf{k}_i^{\mathrm{T}}\mathbf{e}_i + b_i = 1, & i = 1, 2, \ldots, d \\ \mathbf{k}_i^{\mathrm{T}}\mathbf{e}_{j\neq i} + b_i = 0, & i = 1, 2, \ldots, d; \quad 1 \le j \le d. \end{cases} \tag{13}$$

The number of elements in $\mathbf{k}_i$, i.e., N (the number of bands, usually over 100), is very large, while the number of endmembers d is often small (less than seven). It means that (13) is considerably underdetermined. In this case, the following way is presented to overcome the problem. Denote

$$\begin{aligned} &\mathbf{v}_i = \mathbf{e}_i - \mathbf{e}_{i-1}, \qquad i = 1, 2, \ldots, d-1 \\ &\mathbf{V} = [\mathbf{v}_1, \mathbf{v}_2, \ldots, \mathbf{v}_{d-1}]. \end{aligned} \tag{14}$$

It can be seen that the space Γ linearly composed of all the d endmembers with sum-to-one abundances is the $(d-1)$-dimensional space spanned by all the $d-1$ column vectors in matrix $\mathbf{V}$ and that the space Γ_B linearly composed of all the d endmembers with FC abundances is the $(d-1)$-dimensional bounded space formed by all the d vertexes of endmembers $\mathbf{e}_1, \mathbf{e}_2, \ldots, \mathbf{e}_d$. Γ_B is a bounded part in Γ. Then, the following facts hold according to the least squares estimation principle.

1) The nature of the ASC least squares estimation of $\mathbf{s}_0$ by all the d endmembers is to seek the point $\mathbf{s}_0^{\Gamma}$ in the $(d-1)$-dimensional space Γ which is the nearest to $\mathbf{s}_0$. In other words, the point $\mathbf{s}_0^{\Gamma}$ is the projection of $\mathbf{s}_0$ onto Γ, and the ASC least squares estimation results of $\mathbf{s}_0^{\Gamma}$ should be the same as that of $\mathbf{s}_0$.
2) The nature of the FCLS estimation of $\mathbf{s}_0$ by all the d endmembers is to seek the point $\mathbf{s}_0^{\Gamma_B}$ in the $(d-1)$-dimensional simplex Γ_B which is the nearest to $\mathbf{s}_0$ in the bounded space. The FCLS estimation results of $\mathbf{s}_0^{\Gamma_B}$ should be the same as that of $\mathbf{s}_0$.

As can be seen from the aforementioned descriptions, $\mathbf{s}_0$ should have the same signed distance in (12) as its projection $\mathbf{s}_0^{\Gamma}$ in space Γ in terms of the least squares criterion, i.e., the projection error $\mathbf{s}_0^{\Gamma_\perp}$ $(\mathbf{s}_0^{\Gamma_\perp} = \mathbf{s}_0 - \mathbf{s}_0^{\Gamma})$ should have no effect

on distance (12). In this case, super slope $\mathbf{k}_i$ $(i = 1, 2, \ldots, d)$ should be orthogonal to the projection error space $\Gamma_\perp$ formed by all the projection error vectors; then, $\mathbf{k}_i$ $(i = 1, 2, \ldots, d)$ must lie in the space Γ, which can be expressed as

$$\mathbf{k}_i = \sum_{j=1}^{d-1} \beta_i^j \mathbf{v}_i = \sum_{j=1}^{d-1} \beta_i^j (\mathbf{e}_i - \mathbf{e}_{i+1}) = \mathbf{V}\boldsymbol{\beta}_i, \qquad i = 1, 2, \ldots, d \tag{15}$$

where $\boldsymbol{\beta}_i = [\beta_i^1, \beta_i^2, \ldots, \beta_i^{d-1}]^{\mathrm{T}}$ $(i = 1, 2, \ldots, d)$. By putting (15) into (12), we get

$$(\mathbf{E}^{\mathrm{T}}\mathbf{V})\boldsymbol{\beta}_i + b_i\mathbf{1} = \mathbf{y}_i, \qquad i = 1, 2, \ldots, d \tag{16}$$

where $\mathbf{1}$ is a d-dimensional column vector with "1" being its elements and $\mathbf{y}_i$ $(i = 1, 2, \ldots, d)$ is a d-dimensional column vector in which the ith element is 1 and the other elements are 0. Formula (16) can also be expressed as a matrix form as follows:

$$(\mathbf{e}^{\mathrm{T}}\mathbf{V}, \mathbf{1}) \begin{bmatrix} \boldsymbol{\beta} \\ \mathbf{b} \end{bmatrix} = \mathbf{I} \quad \text{or} \quad \begin{bmatrix} \boldsymbol{\beta} \\ \mathbf{b} \end{bmatrix} = (\mathbf{e}^{\mathrm{T}}\mathbf{V}, \mathbf{1})^{-1} \tag{17}$$

where $\boldsymbol{\beta} = [\boldsymbol{\beta}_1, \boldsymbol{\beta}_2, \ldots, \boldsymbol{\beta}_d]$, $\mathbf{b} = [b_1, b_2, \ldots, b_d]$, and $\mathbf{I}$ is a $d \times d$ unit matrix. Furthermore, (15) can also be expressed as follows:

$$\mathbf{k} = [\mathbf{k}_1, \mathbf{k}_2, \ldots, \mathbf{k}_d] = \mathbf{V}\boldsymbol{\beta}. \tag{18}$$

Now, all the distance formulas $f_i(\bullet)$ $(i = 1, 2, \ldots, d)$ are obtained. It can be seen that the following facts hold.

1) $f_i(\mathbf{e}_i) = 1$ and $f_i(\mathbf{e}_{j \neq i}) = 0$, where $i = 1, 2, \ldots, d$ and $1 \leq j \leq d$.
2) The projection error vector $\mathbf{s}_0^{\Gamma_\perp}$ $(\mathbf{s}_0^{\Gamma_\perp} = \mathbf{s}_0 - \mathbf{s}_0^{\Gamma})$ of pixel $\mathbf{s}_0$ has no effect on the distance of $\mathbf{s}_0$, i.e.,

$$f_i(\mathbf{s}_0) = f_i\left(\mathbf{s}_0^{\Gamma} + \mathbf{s}_0^{\Gamma_\perp}\right) = f_i\left(\mathbf{s}_0^{\Gamma}\right). \tag{19}$$

3) When $\sum_{j=1}^{d} \lambda_j = 1$, the following equation holds:

$$f_i\left(\sum_{j=1}^{d} \lambda_j \mathbf{e}_j\right) = \lambda_j \sum_{j=1}^{d} f_i(\mathbf{e}_j). \tag{20}$$

The aforementioned properties completely show that the proposed distance measure is valid for least squares LSMA. The proposed distance is a signed measure, with very low complexity. Furthermore, it is not limited by data dimensionality. The d abundances of pixel $\mathbf{s}_0$ will be given by the d distances as follows:

$$\begin{aligned} \mathbf{P} &= [p_1, p_2, \ldots, p_d]^{\mathrm{T}} \\ &= \left[\frac{f_1(\mathbf{s}_0)}{f_1(\mathbf{e}_1)}, \frac{f_2(\mathbf{s}_0)}{f_2(\mathbf{e}_2)}, \ldots, \frac{f_d(\mathbf{s}_0)}{f_d(\mathbf{e}_d)}\right]^{\mathrm{T}} \\ &= [f_1(\mathbf{s}_0), f_2(\mathbf{s}_0), \ldots, f_d(\mathbf{s}_0)]^{\mathrm{T}}. \end{aligned} \tag{21}$$

It should be noted that the distance is not identical to the traditional Euclidean distance but proportional to the Euclidean distance by its absolute value, and this is adequate for our purpose.

TABLE I
PROPERTY COMPARISON OF DIFFERENT GEOMETRIC MEASURES

	Type	Limited by dimensionality	Complexity
Volume in (1)	Positive	No	Very high
Volume in (3)	Signed	Yes	Very high
Dist. in (7)	Signed	Yes	Low
Dist. in (8)	Positive	No	High
Proposed Dist.	Signed	No	Very low

2) Comparison With Other Measures: The complexity of these measures can be analyzed from the corresponding formula. Compared with large number of pixels to be unmixed, the complexity of the once-for-all computation that is independent of each pixel can be omitted, such as the computation of Vol_0 in (2), the denominator in (3), $\boldsymbol{\alpha}$ in (6), and the process of the distance construction in (7). While, for dimension reduction, its complexity must be properly considered since it is implemented for each pixel, for the distance measure in (8) and the proposed measure, it is analyzed in the original space, since they can be implemented in any dimensional space, and dimension reduction has no benefit for them. In an N-dimensional space, when we unmix one pixel by d endmembers, the proposed measure needs $d \times N$ times of product, the distance in (7) needs $d \times (N + d)$ times of product, in which $d \times N$ times of product are due to dimensionality reduction, and the distance in (8) needs $d \times N^2$ times of product. Both the volume in (1) and the volume in (3) have very high complexity of $O(d^3)$, added by that of dimension reduction. It is seen that the proposed measure has the lowest complexity. The other properties of each measure have already been pointed out after the description of each measure. All the properties are shown in Table I.

B. Construction of Geometric FCLS-LSMA Method

In this section, we suppose that all pixels that lie in the plane Γ can be spanned by all endmembers, and after, the projection error vectors have no effect on the geometric unmixing analysis based on the proposed distance. We call an endmember a positive/negative one if the corresponding abundance is positive/negative in current unmixing and call an endmember combination the optimal one if it corresponds to the optimal FCLS-LSMA.

For pixel $\mathbf{s}_0$, if it lies in the simplex Γ_B bounded by all the endmember vertexes, then the fractional abundances of pixel $\mathbf{s}_0$ obtained by each former geometric measure are FC, and the results are optimal in terms of the least squares criterion. When mixed pixel $\mathbf{s}_0$ is outside of the simplex Γ_B, the case is not true. For the signed measure, some fractional abundance(s) will be of negative value(s), while for the positive measure, the sum of abundances will be larger than one. This kind of pixel exists widely and needs to be processed properly. Once the geometric method based on the proposed measure or any other measures could not get the optimal FCLS unmixing results, then how

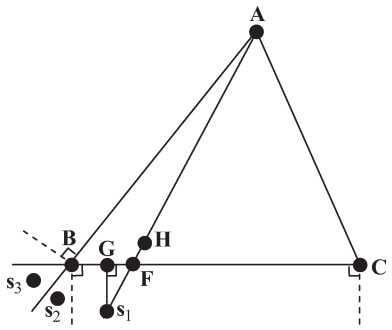

Fig. 2. Diagram of finding the optimal FCLS estimation.

to get the optimal FCLS solution or to implement a geometric FCLS-LSMA?

In Fig. 2, unmixing by three endmembers is considered. If the unmixing results of a pixel unmixed by $\mathbf{A}$, $\mathbf{B}$, and $\mathbf{C}$ meet the full-constraint requirement, the pixel must lie in triangle $\mathbf{ABC}$, and the corresponding unmixing result is optimal. The positions of three pixels $\mathbf{s}_1$, $\mathbf{s}_2$, and $\mathbf{s}_3$ outside of triangle $\mathbf{ABC}$ are shown in Fig. 2. When there is one endmember corresponding to a negative abundance, as for pixels $\mathbf{s}_1$ and $\mathbf{s}_2$, the abundance is reset to zero, and the other two endmembers are then further used for its next unmixing. Note that the reset is strictly in line with the FCLS criterion. The endmembers corresponding to zero abundances are checked out first, and then, they need not to participate in further unmixing. It also should be noted that the case is different from any endmember selection methods for unmixing, in which some endmembers are abandoned and do not calculate abundances for them at all, no matter they correspond to zero abundances or not in terms of the least squares criterion. When there are two negative endmembers, for example, $\mathbf{A}$ and $\mathbf{C}$, as for pixel $\mathbf{s}_3$, the two-endmember combinations $(\mathbf{A}, \mathbf{B})$ and $(\mathbf{B}, \mathbf{C})$ should be considered for the second unmixing. If the unmixing result corresponding to a two-endmember combination, for example, $(\mathbf{B}, \mathbf{C})$, meets the full constraint, as for pixel $\mathbf{s}_1$, the result is optimal. If none of the two-endmember combinations considered provides a group of FC abundances, as for pixels $\mathbf{s}_2$ and $\mathbf{s}_3$, there must be only one positive endmember (i.e., endmember that corresponds to a positive abundance) all the time, and the pixel should be ascribed to the endmember with 100% abundance.

In Fig. 2, when pixel $\mathbf{s}_1$ is first unmixed by a signed-measure-based geometric method, endmember $\mathbf{A}$ is then attached by a negative abundance. The corresponding unmixing error vector is $\mathbf{0}$, but the negative constraint is not meet. If the negativity abundance is reevaluated to zero and each positive abundance is divided by the sum of two positive abundances, then the new abundances are FC. It can be calculated that the corresponding unmixing error is $|\mathbf{Fs}_1|$. If a positive-measure-based geometric method is used for the first unmixing and the abundances are reevaluated, if necessary, to be FC, it can also be calculated that the unmixing error vector is $\mathbf{Hs}_1$, where $\mathbf{H}$ satisfies $|\mathbf{FH}| = |\mathbf{Fs}_1| \times |\mathbf{AF}|/(|\mathbf{AF}| + 2|\mathbf{Fs}_1|)$. For a signed-measure-based method, as the proposed method, if the pixel $\mathbf{s}_1$ is unmixed by two positive endmembers $\mathbf{B}$ and $\mathbf{C}$, the least squares optimal solution is then obtained, with unmixing error vector $\mathbf{Gs}_1$. Obviously, $\mathbf{G}$ is the optimal FCLS estimation for $\mathbf{s}_1$.

When pixel $\mathbf{s}$ is unmixed by three endmembers, for example, $\mathbf{A}$, $\mathbf{B}$, and $\mathbf{C}$, the optimal unmixing process can be simplified as follows.

1) Three endmembers are used in the first unmixing. If the unmixing abundances are FC, the results are optimal. If there are two negative endmembers, for example, $\mathbf{A}$ and $\mathbf{B}$, and the inner angle $\mathbf{ACB}$ is acute, then pixel $\mathbf{s}$ can be directly attributed to the positive endmember $\mathbf{C}$ with 100% abundance. In this case, only one unmixing is required for pixel $\mathbf{s}$.
2) If there is only one negative endmember, for example, $\mathbf{A}$, in the first unmixing, then the other two positive endmembers are used for the second unmixing. If the second unmixing abundances are FC, then the results are optimal. If not, the mixed pixel can be directly attributed to the positive endmember with 100% abundance. In this case, unmixing is needed to run twice for the pixel.
3) If there are two negative endmembers, for example, $\mathbf{A}$ and $\mathbf{B}$, in the first unmixing and the inner angle $\mathbf{ACB}$ is obtuse, then endmember combinations $(\mathbf{A}, \mathbf{C})$ and $(\mathbf{B}, \mathbf{C})$ are used to unmix pixel $\mathbf{s}$ in turn. Only one of the results with FC unmixing abundances is optimal. In this case, twice or three times unmixing is enough.

In fact, most and even all of the angles are often acute. These cases will simplify the FC adjusting to some degree. The computation of angles is independent of mixed pixels, and its complexity, therefore, can be omitted. In summary, our method will be very fast and can provide the optimal results meanwhile.

Before construction of the geometric FCLS-LSMA method based on our proposed measure in an N-dimensional space, the following facts should be addressed.

First, for d-endmember unmixing, if there is only one negative endmember, it must not be included in optimal endmember combinations.

Second, if there is more than one m-endmember combination with full-constraint requirements and any endmember combination with more than m endmembers does not meet the requirement, then there must be one and only one m-endmember combination that corresponds to the optimal FCLS solution.

Third, for d-endmember unmixing, if there is more than one negative endmember, some of them may still be included in optimal endmember combinations.

Fourth, if there are d_0 negative endmembers in a d-endmember combination, then the d_0 $(d-1)$-endmember combinations can be formed by deleting each negative endmember in the d-endmember combination. Then, there is, at most, one $(d-1)$-endmember combination that is the optimal endmember combination.

Finally, if more than one of the m-endmember combinations are generated from different $(m+1)$-endmember combinations, then there may be two or more m-endmember combinations that correspond to FC abundances.

Perhaps, the fourth case is difficult to understand for readers. We show the case in Fig. 3. For four endmembers, supposing that $\mathbf{A}$ and $\mathbf{C}$ are negative endmembers for unmixing pixel $\mathbf{s}$, then pixel $\mathbf{s}$ must lie in the space spanned by $\mathbf{BF}$, $\mathbf{BE}$, $\mathbf{BD}$,

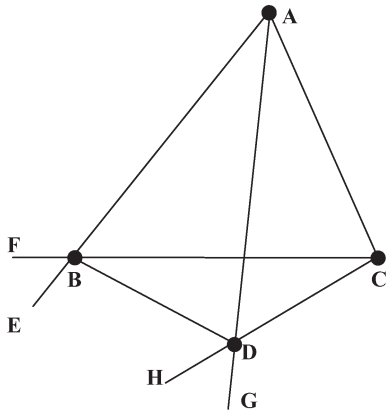

Fig. 3. Diagram of finding the only-three-endmember combination corresponding to FC abundances.

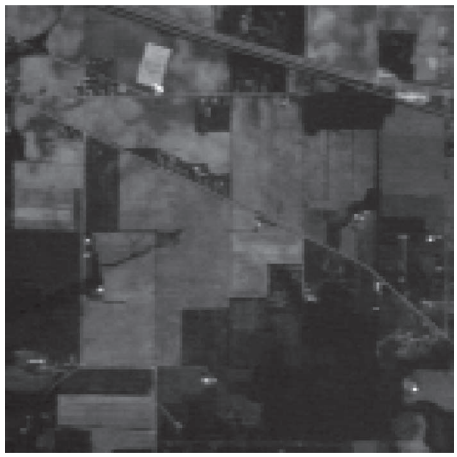

Fig. 4. Band 100 of the hyperspectral imagery used.

$\mathbf{DG}$, and $\mathbf{DH}$. When the included angle θ between plane $\mathbf{ABD}$ and plane $\mathbf{CBD}$ is acute, both the two corresponding three-endmember combinations, i.e., $(\mathbf{A}, \mathbf{B}, \mathbf{D})$ and $(\mathbf{C}, \mathbf{B}, \mathbf{D})$, do not meet the full-constraint requirements. When the angle θ is obtuse, only one of the two 3-endmember combinations meets the full-constraint requirements. Furthermore, if $\mathbf{D}$ is also a negative endmember, then according to the aforementioned analysis, at most one 3-endmember combination corresponds to FC abundances in any two 3-endmember combinations, and therefore, at most one 3-endmember combination corresponds to FC abundances in all the three-endmember combinations. The analysis can be extended to a higher space with more endmembers.

Based on the aforementioned facts, for unmixing a pixel $\mathbf{s}$ by d endmembers, the steps of the proposed geometric FCLS-LSMA are listed as follows.

Step 1) Pixel $\mathbf{s}$ is unmixed by all the d endmembers first. If the resulted abundances are FC, the unmixing is finished. Otherwise, the processing goes into the next step.

Step 2) If there are d_1 negative abundances in step 1, then d_1 $(d-1)$-endmember combinations are formed by removing each of the negative endmembers from the d-endmember combination. Then, $\mathbf{s}$ is unmixed by each $(d-1)$-endmember combination in turn. If the resulted abundances according to the ith $(d-1)$-endmember combination are FC, the unmixing is finished, and if all the d_1 times of unmixing results do not meet with full-constraint requirements, the processing goes into the next step.

Step 3) All the d_2 $(d-2)$-endmember combinations are formed for each unmixing in step 2 by removing each of the negative endmembers. Then, the pixel $\mathbf{s}$ is unmixed by each $(d-2)$-endmember combination in turn. If one or more unmixing results meet with full-constraint requirements, the optimal unmixing can be obtained from them by comparing the unmixing errors, and if none of the unmixing abundances is FC, the processing goes into the next step.

Step 4) The processing is continued until two-endmember combinations are considered. If all the unmixing results of two-endmember combinations do not meet with full-constraint requirements, the mixed pixel is ascribed to one of the generated endmembers with 100% abundance by comparing the unmixing residual errors. At the end of the analysis, the abundances of the endmembers out of the optimal endmember combination are set to zero.

After this process, the optimal result of FCLS-LSMA can be obtained with a low complexity. The geometric unmixing is quite different from iterative unmixing methods, although it may unmix several times for one pixel. Some comparisons of unmixing residual errors are used in steps 3 and 4. They increase the computational cost. If the first presented unmixing meeting with the full-constraint requirement is viewed as the "optimal" result, the corresponding method will be completely free of comparing of the unmixing errors and will be very fast, with a suboptimal result, as shown in experiments.

IV. Experiments and Results

The Airborne Visible Infrared Imaging Spectrometer (AVIRIS) data acquired in the Indian Pine test site (145×145 pixels and 200 bands) in 1992 were used for testing (Fig. 4). It covers an agriculture/forestry landscape, in which 16 classes are included [22]. The processor of the computer is an Intel Pentium 4 Dual CPU at 1.60 GHz. Here, the traditional iterative Quadratic Programming (QP) method in [10], the iterative method in [11] and [12], the geometric method in [13], the geometric method in [17], and the proposed geometric method were briefly named the I-QP, I-Heinz, G-Geng, G-Luo, and G-Wang methods, respectively. When the abundances obtained by the G-Geng or G-Luo method are not FC, they were then adjusted to meet ASC and ANC.

The first group of experiments aims to compare the complexities in terms of running time. The 16 endmembers were obtained by averaging the 16 classes' spectra. One hundred thousand mixed pixels were linearly composed with random generated abundances for each endmember combination. The number of endmembers in these combinations increased from 2

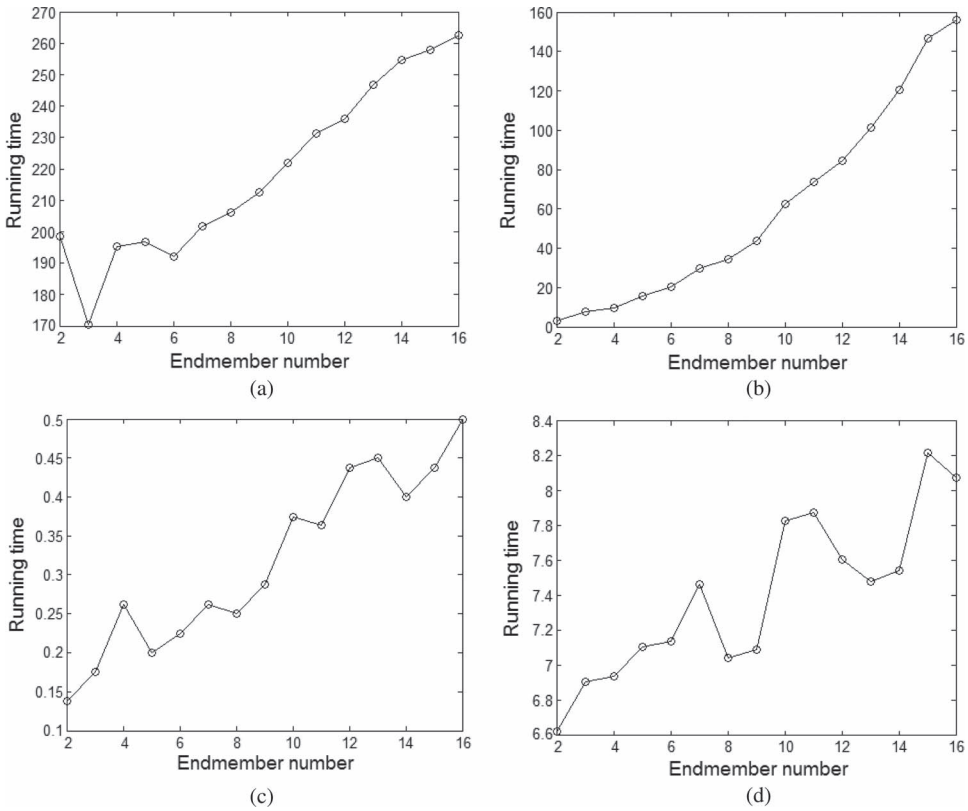

Fig. 5. Comparison of running times (in seconds). (a) I-QP method. (b) G-Geng method. (c) G-Wang method. (d) I-Heinz method.

to 16. The I-QP, I-Heinz, G-Geng, and G-Wang methods were compared with each other. Some methods listed in Section II were not used in the comparison, since their complexities have a simple relation to one of the three methods selected above. The executed time for each method is shown in Fig. 5. They are plotted in three separated subfigures for their great difference. We can see that our method speeded up the traditional method by more than 400 times. The mean unmixing time for one pixel is between 10^{-6} and 10^{-7} s. The G-Geng method improved the speed from two to a couple of ten times. Each method provided nearly zero unmixing error since the artificially synthesized mixed data all lie in the interior of the convex bounded by all the endmember vertexes.

The runtime curves in Fig. 5(a), (c), and (d) are not strictly monotonic with the increasing of the endmember number. The reason is that an iteration-based method is affected by some stochastic factors, such as initialization, termination condition, and local optimization, while a geometry-based method is affected by data distribution. The method shown in Fig. 5(b) is also affected by the distribution factor, but its geometry computation dominates the running time, which has a very high complexity of $O(d^3)$, leading to a strictly monotone runtime curve.

The second experiment was carried out for comparison of the unmixing errors. Each set of 1000 pixels was selected from the three largest sizes of classes, respectively. They were used to randomly synthesize 1000 mixed pixels. There must be some synthesized pixels outside of the convex for the spectral variability of each class. The G-Geng, G-Luo, I-Heinz, I-QP, and G-Wang methods were compared with each other. The

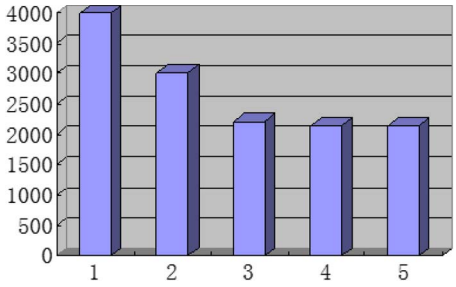

Fig. 6. Comparison of unmixing errors. (Abscissa) (1) G-Geng method, (2) G-Luo method, (3) I-Heinz method, (4) I-QP method, and (5) G-Wang method. (Ordinate) Unmixing error.

mean of the least squares unmixing error was used for the evaluation

$$\frac{1}{N}\sum_{j=1}^{N}\sqrt{\varepsilon_j^{\mathrm{T}}\varepsilon_j}=\frac{1}{N}\sum_{j=1}^{N}\sqrt{(\mathbf{s}_j-\mathbf{e}\times\mathbf{P}^j)^{\mathrm{T}}(\mathbf{s}_j-\mathbf{e}\times\mathbf{P}^j)}. \quad (22)$$

The results are shown in Fig. 6. It indicates that the I-QP and G-Wang methods provide the minimum unmixing error, which is 2149. The result is in line with the theory analysis that our method can get the theoretically optimal solution. Specifically, the I-Heinz method gets a slightly greater unmixing error than the I-QP and G-Wang methods, since it is designed as a suboptimal method. The G-Geng and G-Luo methods have the worst performances, since obtaining FC abundances for them does not meet the least squares criterion.

The execution times of the I-QP, I-Heinz, and G-Wang methods are 12.0000, 1.5470, and 0.0470 s, respectively.

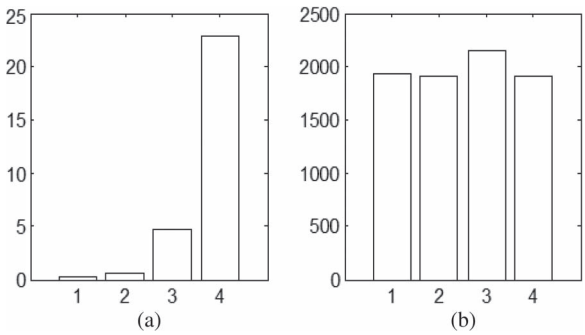

Fig. 7. Comparison of running times and unmixing errors. (Abscissa) (1) SG-Wang method, (2) OG-Wang method, (3) I-Heinz method, and (4) I-QP method. (Ordinate) (a) Running time (in seconds) and (b) unmixing error.

In the third experiment, the number of classes was increased to five, i.e., all the pixels are selected from the five largest sizes of classes. Here, the G-Wang method was divided into optimal G-Wang method (OG-Wang method) and suboptimal G-Wang method (SG-Wang method) with the consideration that comparison of unmixing errors was used. The comparisons of running times and unmixing errors are shown in Fig. 7. It can be seen that the I-QP method gets the optimal solution, as the OG-Wang method does, but it is very slow. Although the I-Heinz method is faster than the I-QP method, it is slower than the G-Wang methods and with greater errors. It also shows that the SG-Wang method still has low unmixing error with the least running time, 0.2739 s, while the OG-Wang method has fast speed with the lowest unmixing error, 1902. The two G-Wang methods provide us a selection for different purposes. The running time and unmixing error are shown in Fig. 7.

In the last experiment, the averaged absolute abundance error criterion was used to evaluate the proposed method in a real hyperspectral unmixing case

$$\frac{1}{dN}\sum_{i=1}^{d}\sum_{j=1}^{N}\left|P_i^j-\tilde{P}_i^j\right| \tag{23}$$

where $\tilde{P}_i^j$ is the ith true abundance of the jth pixel and P_i^j is the ith calculated one. In order to make an evaluation, we unmix all the pure pixels of the three largest sizes of classes. The I-QP, I-Heinz, G-Geng, and G-Wang methods are compared. The fractional errors are 0.3520, 0.2250, 0.2250, and 0.2235 for the G-Geng, G-Wang, I-QP, and I-Heinz methods, respectively. The fractional images are shown in Fig. 8. The proposed G-Wang method and the I-QP method obtain the same results again. From this experiment, we can see that, although the G-Wang and I-QP methods are superior to the I-Heinz method in terms of the least squares criterion, they are slightly inferior to the I-Heinz method when fractional abundances are considered.

V. Conclusion

This paper has proposed a geometric FCLS-LSMA method based on a new distance measure. There are two major advantages over the iteration-based FCLS-LSMA method. One is that the geometric method avoids huge times of iterations.

Fig. 8. Fractional images. (Line 1) Truth images. (Line 2) G-Geng method. (Line 3) G-Luo method. (Line 4) I-Heinz method. (Line 5) G-Wang method and I-QP method. (Column 1) Class 2. (Column 2) Class 11. (Column 3) Class 14.

The other advantage is to provide intuitionistic information for us. Owing to the intuitionistic information, the proposed method can be implemented FC, and therefore, the optimal least squares results can be obtained. The proposed method has low complexity and is free of dimension reduction with the help of the simple distance measure. Experiments show that the proposed method can obtain the same optimal FCLS solution as the traditional iteration-based FCLS-LSMA; meanwhile, it is much faster than the other distance-based methods tested, particularly the iteration-based method.

When a mixed pixel is exterior to the simplex formed by the vertexes of the total endmembers, the endmembers strictly corresponding to zero fractional abundances are removed from the further solving processing in turn. In this case, the main solving procedure in this special case can be viewed as an optimal endmember selection in terms of the least squares criterion.

It should be noted that the proposed method meets the least squares criterion, and hence, it is optimal in terms of minimizing the two-norm of the unmixing residual. However, it does not mean that the proposed method is optimal when a fractional abundance criterion is considered. In further work, we will seek for the combination of our geometric approach with highly accurate unmixing methods, such as methods based on multiple-endmember spectral mixture analysis.

REFERENCES

[1] Y. Yan, Y. Zhao, H.-F. Xue, X.-D. Kou, and Y. Liu, "Integration of spatial–spectral information for hyperspectral image classification," in *Proc. 2nd IITA-GRS*, 2010, vol. 1, pp. 242–245.

[2] J. B. Adams and M. O. Smith, "Spectral mixture modeling: A new analysis of rock and soil types at the Viking lander 1 suite," *J. Geophys. Res.*, vol. 91, no. B8, pp. 8098–8112, Jul. 10, 1986.

[3] S. Jia and Y. Qian, "Spectral and spatial complexity-based hyperspectral unmixing," *IEEE Trans. Geosci. Remote Sens.*, vol. 45, no. 12, pp. 3867–3879, Dec. 2007.

[4] A. Plaza, P. Martinez, R. Perez, and J. Plaza, "A quantitative and comparative analysis of endmember extraction algorithms from hyperspectral data," *IEEE Trans. Geosci. Remote Sens.*, vol. 42, no. 3, pp. 650–663, Mar. 2004.

[5] M. Brown, H. Lewis, and S. Gunn, "Linear spectral mixture models and support vector machine for remote sensing," *IEEE Trans. Geosci. Remote Sens.*, vol. 38, no. 5, pp. 2346–2360, Sep. 2000.

[6] J. Li and L. M. Bruce, "Wavelet-based feature extraction for improved endmember abundance estimation in linear unmixing of hyperspectral signals," *IEEE Trans. Geosci. Remote Sens.*, vol. 42, no. 3, pp. 644–649, Mar. 2004.

[7] Y. E. Shimabukuro and J. A. Smith, "The least-squares mixing models to generate fraction images derived from remote sensing multispectral data," *IEEE Trans. Geosci. Remote Sens.*, vol. 29, no. 1, pp. 16–20, Jan. 1991.

[8] J. Boardman, "Inversion of high spectral resolution data," in *Proc. SPIE*, 1990, vol. 1298, pp. 222–233.

[9] Y. E. Shimabukuro, "Shade images derived from linear mixing models of multispectral measurements of forested areas," Ph.D. dissertation, Dept. Forest Wood Sci., Colorado State Univ., Fort Collins, CO, 1987.

[10] J. J. Settle and N. A. Drake, "Linear mixing and estimation of ground cover proportions," *Int. J. Remote Sens.*, vol. 14, no. 6, pp. 1159–1177, Apr. 1993.

[11] D. C. Heinz and C.-I. Chang, "Fully constrained least squares linear spectral mixture analysis method for material quantification in hyperspectral imagery," *IEEE Trans. Geosci. Remote Sens.*, vol. 39, no. 3, pp. 529–545, Mar. 2001.

[12] D. Heinz, C.-I. Chang, and M. L. G. Althouse, "Fully constrained least squares-based linear unmixing," in *Proc. Int. Geosci. Remote Sens. Symp.*, Hamburg, Germany, 1999, pp. 1401–1403.

[13] X. Geng, B. Zhang, X. Zhang, and L. Zheng, "An unmixing method of hyperspectral imagery based on convex volume in high dimensional space," (in Chinese), *Prog. Nat. Sci.*, vol. 14, no. 7, pp. 810–814, 2004.

[14] M. Zortea and A. Plaza, "A quantitative and comparative analysis of different implementations of N-FINDR: A fast endmember extraction algorithm," *IEEE Geosci. Remote Sens. Lett.*, vol. 6, no. 4, pp. 787–791, Oct. 2009.

[15] L. Wang, X. Jia, and Y. Zhang, "A novel geometric algorithm of feature selection for hyperspectral imagery," *IEEE Geosci. Remote Sens. Lett.*, vol. 4, no. 1, pp. 171–175, Jan. 2007.

[16] L. Wang and Y. Zhang, "Speed-up for N-FINDR algorithm," *J. Harbin Inst. Technol.*, vol. 15, no. 1, pp. 141–144, 2008, (New Series).

[17] W. Luo, L. Zhong, B. Zhang, and L.-R. Gao, "Subspace distance based spectral unmixing method for hyperspectral imagery," (in Chinese), *Prog. Nat. Sci.*, vol. 18, no. 10, pp. 1175–1180, 2008.

[18] I. T. Jolliffe, *Principal Component Analysis*. New York: Springer-Verlag, 1986.

[19] X. Liu, L. Gao, B. Zhang, X. Zhang, and W. Luo, "An improved MNF transform algorithm on hyperspectral images with complex mixing ground objects," in *Proc. 1st Int. CISP*, 2008, vol. 3, pp. 479–483.

[20] R. Heylen, D. Burazerovic, and P. Scheunders, "Fully constrained least squares spectral unmixing by simplex projection," *IEEE Trans. Geosci. Remote Sens.*, vol. 49, no. 11, pp. 4112–4122, Nov. 2011.

[21] L. Wang and X. Jia, "Integration of soft and hard classification using extended support vector machines," *IEEE Geosci. Remote Sens. Lett.*, vol. 6, no. 3, pp. 543–547, Jul. 2009.

[22] L. David, "Multispectral data analysis: A signal theory perspective," Purdue Univ., West Lafayette, IN, 1998.

Liguo Wang received the M.S. degree and the Ph.D. degree in signal and information processing from the Harbin Institute of Technology, Harbin, China, in 2002 and 2005, respectively.

From 2006 to 2008, he held a postdoctoral research position in the College of Information and Communications Engineering, Harbin Engineering University, Harbin, where he is currently a Professor with research interests in remote sensing and machine learning. He has published one book named *Processing Techniques of Hyperspectral Imagery* and more than 70 papers in journals and conference proceedings.

Danfeng Liu received the B.S. degree from Harbin Engineering University, Harbin, China, in 2009, where she is currently working toward the Ph.D. degree in the College of Information and Communications Engineering.

Her research interests include hyperspectral image display and remote sensing image processing.

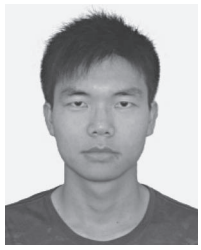

Qunming Wang received the B.S. and M.S. degrees from Harbin Engineering University, Harbin, China, in 2010 and 2012, respectively. He is currently working toward the Ph.D. degree in the Department of Land Surveying and Geo-Informatics, The Hong Kong Polytechnic University, Kowloon, Hong Kong.

His current research interests focus on remote sensing image analysis and pattern recognition.